**Geomechanics and Engineering**, *Vol. 24, No. 3 (2021) 215-226*
DOI: https://doi.org/10.12989/gae.2021.24.3.215


# Analysis of the crack propagation rules and regional damage characteristics of rock specimens

Yangyang Li[1], Yadong Xu[1], Shichuan Zhang*[1], Jing Fan[2], Guobin Du[2], Lu Su[2] and Guangsheng Fu[3]

[1]*School of Energy and Mining Engineering, Shandong University of Science and Technology, No.579 Qianwangang Road, Huangdao District, Qingdao, Shandong Province, 266590, China*
[2]*Shandong Energy Mining Group Co., Ltd, No.69, Business Street Road, Luozhuang District, Linyi, Shandong Province, 276017, China*
[3]*Shandong Bureau of China Metallurgical Geology Bureau, No.88, Chunyang Road, Chengyang District, Qingdao, Shandong Province, 266109, China*

*(Received October 21, 2020, Revised January 9, 2021, Accepted January 15, 2021)*

**Abstract.** To study the evolution mechanism of cracks in rocks with multiple defects, rock-like samples with multiple defects, such as strip-shaped through-going cracks and cavity groups, are used, and the crack propagation law and changes in AE (acoustic emission) and strain of cavity groups under different inclination angles are studied. According to the test results, an increase in the cavity group inclination angle can facilitate the initial damage degree of the rock and weaken the crack initiation stress; the initial crack initiation direction is approximately 90°, and the extension angle is approximately 75~90° from the strip-shaped through-going cracks; thus, the relationship between crack development and cavity group initiation strengthens. The specific performance is as follows: when the initiation angle is 30°, the cracks between the cavities in the cavity group develop relatively independently along the parallel direction of the external load; when the angle is 75°, the cracks between the cavities in the cavity group can interpenetrate, and slip can occur along the inclination of the cavity group under the action of the shear mechanism rupture. With the increase in the inclination angle of the cavity group, the AE energy fluctuation frequency at the peak stress increases, and the stress drop is obvious. The larger the cavity group inclination angle is, the more obvious the energy accumulation and the more severe the rock damage; when the cavity group angle is 30° or 75°, the peak strain of the local area below the strip-shaped through-going fracture plane is approximately three times that when the cavity group angle is 45° and 60°, indicating that cracks are easily generated in the local area monitored by the strain gauge at this angle, and the further development of the cracks weakens the strength of the rock, thereby increasing the probability of major engineering quality damage. The research results will have important reference value for hazard prevention in underground engineering projects through rock with natural and artificial defects, including tunnels and air-raid shelters.

**Keywords:** rock-like materials; multiple defects; cavity group; crack propagation; regional damage

## 1. Introduction

Rock masses often contain natural structural defects such as joints, faults and underground waterways (Madkour 2012). With the construction of mines and underground engineering, the number of structural defects in natural rock masses further increases, resulting in a phenomenon in which natural structural defects and artificial structural defects coexist. Defects are very harmful during rock engineering, and they often cause disasters such as cavern collapse (Qian and Zhou 2018) and water inrush through fissures and redistribute tectonic stress (Aalianvari 2017). For this reason, scholars have increasingly focused on the study of rock damage mechanisms (Kadomtsev *et al.* 2011) and have successively carried out a large number of experimental studies on the changes in mechanical behaviour caused by the internal defects of rock masses and made phased progress (Shemirani *et al.* 2017), which is very helpful for understanding engineering problems such as the crack propagation mechanism of surrounding rock with multiple defects (Vahab and Hadi 2016).

Among the many methods available for researching prefabricated defects in rock masses, many scholars have focused on numerical simulations and laboratory experiments. In terms of numerical simulation, Lee and Jeon (2010) used PFC2D (Particle Flow Code in 2D) to conduct a systematic numerical simulation study on the cracking behaviour of a specimen with two nonparallel cracks under uniaxial compression and believed that the interpenetration of the two cracks is mainly affected by the crack angle and material. Moir *et al.* (2009) used numerical simulation software to include more than 20 joints in a rock mass containing faults and studied how the initial joint mode affects the evolution of the trajectory of the fault zone. Zeng *et al.* (2018) established a simplified sample model with different hole shapes and pointed out that the change in hole shape has little effect on the deformation ability of the sample but will result in different influence rules on the strength characteristics and failure modes of the sample. Yang and Huang (2014) further studied the influence of fracture dip angle on the mechanical parameters and crack growth characteristics of dual-porosity fractured samples through micromechanics tests

*Corresponding author, Ph.D.
E-mail: 373260186@qq.com



ISSN: 2005-307X (Print), 2092-6219 (Online)

and particle flow simulations. Liang *et al.* (2012) used RFPA3D (Rock Failure Process Analysis in 3D) to discuss the propagation of three-dimensional cracks in heterogeneous rock with different prefabricated defects and analysed the fracture process of defects at the rock surfaces. Although numerical simulation can overcome many disadvantages of real rock testing (Bahaaddini *et al*. 2013, Mejia Camones *et al*. 2013), such as a high cost, long experimental time, and inaccurate control of a single variable, the rock itself is an anisotropic, discontinuous material, rock mechanical properties are extremely complex and are difficult to describe numerically. Simulation analysis has difficulty meeting the actual needs of engineering (Jin *et al.* 2017, Jaime *et al.* 2015). Therefore, some scholars have analysed the characteristics of rocks containing defects through laboratory tests and obtained informative results. For example, Xu *et al.* (2017) studied the temporal and spatial variation in microcracks in granite with a prefabricated single hole under uniaxial compression by using AE (acoustic emission) technology and the moment tensor analysis method and revealed the correlation between the active area of AE and the macroscopic fracture locations. In the research of Fan *et al.* (2018), by designing a combination of open cracks and holes, it was found that the defect locations and inclinations around holes have a great influence on the crack propagation process and the resulting hole damage. Dyskin *et al.* (2003) used the method of prefabricating three-dimensional cracks in transparent resin materials to study the propagation and interpenetration laws of internal three-dimensional cracks under compression and theoretically explained the propagation and interpenetration of various types of three-dimensional cracks. Regarding uniaxial compression testing with square holes, Zhou *et al.* (2017) proposed that the number and layout of square holes were closely related to the change in the mechanical properties of the specimen, and four fracture modes were observed in the fracture morphology of the specimen. Previous studies have conducted a considerable amount of research on different combinations of one, two or several prefabricated fractures in rock (Alitalesh *et al.* 2020, Haeri *et al.* 2014), and a series of experiments have been carried out on prefabricated holes (Dzik and Lajtai 1996, Haeri *et al.* 2015). Many informative experimental data and conclusions have been obtained.

Rock composites material, as an effective carrier for laboratory rock experiments, has always been the focus of research by relevant scholars. Golewski studied the fracture toughness of concrete under the influences of different factors such as composition, age and mineral additives, providing an important reference method for the accurate mix design of rock composites materials (Golewski and Sadowski 2016, Golewski 2019). For studies on prefabricated cracks and cavity groups in rock-like rock, whether in 2D or 3D or with numerical simulation or laboratory experimentation, the results are mostly focused on the study of a single defect in a rock mass. However, due to the construction of underground engineering, the increase in the number of structural defects in a rock mass often leads to the formation of a complex defective rock mass with an extremely complex spatial distribution of defects. For example, the Longtan Hydropower Station dam (Zhang 2005) site includes 119 underground caverns 30 km in size in a fault-containing rock mass within an area of only 0.6 $km^2$. Hundreds of artificial caves in the weak sandstone below the city centre of the city of Nottingham, UK (Waltham and Swift 2004) caused major geological disasters. A large number of horizontal roadways have been excavated in the water-rich layer between the aquifer and the water barrier in the Asturian Coal Basin (Gonzalez and Fernandez 2019). The Jurong Rock Caverns Project (Winn *et al* 2019) incudes plans to excavate as many as 5 oil storage caverns and roadways in a zone with low-angled bedded meta-sedimentary mudstone. These underground rock mass engineering projects have a large construction volume, and the locations of cross caverns vary. The interaction of natural and artificial defects results in a structure that is extremely complex (Oh *et al.* 2019, Lyer and Podladchikov 2009).

Based on the summary of previous research results, few studies have been conducted on prefabricated multiple defects structure such as strip-shaped through-going cracks and cavity groups in specimens at the same time, and the comprehensive analysis of the rock fracture mechanism caused by the angle change in a cavity group is not sufficient. Therefore, the present paper attempts to simplify structures such as underground working faces or underground river channels into horizontal edge cracks or oblique cracks, and underground tunnels and caverns into holes. Although there is a certain deviation of the results determined with these simplifications and those of actual engineering, such work still has a certain exploration value for the large geological engineering project.

Therefore, this paper adopts the method of analysing strip-shaped through-going cracks and cavity groups together by changing the inclination angle of the cavity group. The overall deformation characteristics, crack propagation law and AE characteristics of rock with multiple defects during uniaxial compression testing are analysed. The fracture mechanism of the local rock between the front end of the prefabricated strip-shaped through-going crack and the upper boundary of the cavity group is studied for various angles of the cavity group. On this basis, the microscopic characteristics of the crack propagation angle are further summarized, which is of great significance for solving the disaster problem in mining and tunnel excavation (Kong *et al.* 2018, Wong *et al.*2001).

## 2. Experimental work

### *2.1 Specimen preparation*

By adding appropriate aggregates and mineral additives, the composite material can be highly homogenized, resulting in smaller internal microcracks (Golewski 2019), which has a great influence on the bearing capacity of the structure. Following relevant research (Kulatilake *et al.* 2001, Shen *et al.* 2015) from studies worldwide, this paper obtained the relationship between the water content and the strength and elastic modulus of the test block through rock mechanics tests. When the proportion of water in the model

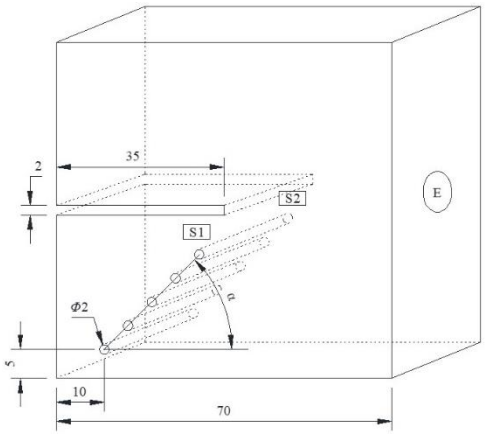


Fig. 1 Schematic drawing of multiple defects (Unit: mm)

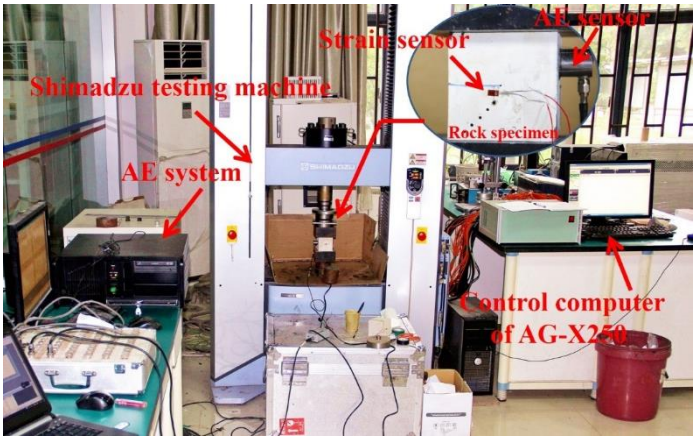


Fig. 2 Loading and monitoring system for tests

plaster reaches 40%, the density of the gypsum specimen is 1.49 g/cm$^3$, and the uniaxial compressive strength reaches 25 MPa. At this time, the damage mode of this type of rock material under uniaxial compression is similar to the original rock on the first layer of a mine and has a more favourable brittleness than it, so this material can effectively simulate the real brittle rock and the crack propagation process.

The specimens were made of gypsum, cement slurry and special additives. The specimens were cubes with a side length of 70 mm, and a 2 mm height and a 35 mm width were made by the cutting method. To investigate the strength, deformation characteristics and fracture evolution of the samples with the change in the inclination angle of the cavity group, a cavity group with a diameter of 2 mm was made under the strip-shaped through-going crack and arranged on the same plane. The included angle between the cavity group and the lower end surface of the specimen was α, which was changed to 30°, 45°, 60° and 75°. The bottom hole is located at the same position in all the specimens, 10 mm from the left boundary and 5 mm from the lower boundary, and the vertical distance between the upper boundary of the cavity group and the strip-shaped through-going crack is 10 mm.

### *2.2 Experimental design*

Considering the influence range of the hole on the stress state of the surrounding rock (3-5 times the hole radius), the spacing between holes is selected to be 7 mm, which can prevent the influence of concentrated stress around the hole on the test error (Mondal *et al*. 2019). Before the start of the test, lubricating oil is smeared on the upper and lower ends of the specimen to prevent the end effect caused by friction between the end face and the loading plate. One strain sensor is arranged in the middle of the section that is closest to the strip-shaped through-going crack and the cavity group, and one strain sensor is arranged on the front and rear surfaces, which are S1 and S2, respectively. They are mainly used to monitor the expansion between the upper end of the cavity group and the lower end of the strip-shaped through-going crack. This setup is used to analyse the relationship between the axial stress and local strain and simultaneously arranges the AE probe at the geometric centre of the right end of the specimen to automatically collect and record the energy amplitude change process in the intensely active area, marked as E. A three-dimensional schematic diagram of the prefabricated defects in the rock-like specimens is shown in Fig. 1.

### *2.3 Experimental equipment*

The test equipment mainly includes an experimental loading system, a strain acquisition system, an AE instrument and a high-speed camera. The experimental

loading system adopts the Shimadzu AG-X250 testing machine, which has high data collection accuracy and good stability. The maximum loading load is 250 kN. The test uses displacement control to apply the load, and the loading speed is 0.005 mm/s. The sensitivity of the testing machine is set to 80%, that is, when the axial bearing pressure is reduced by 80% of the compressive strength, the testing machine will automatically stop. Strain data were collected by the DH-3816N strain acquisition system, and the sampling interval was 60 points/min. The strain sensor was a BX120-3AA strain gauge: the base size was 7.3 mm×4.1 mm, the wire grid size was 3.0×3.1 mm, the strain limit was 20000 μm/m, and the sensitivity coefficient was 2.0±1%.
The AE instrument adopts the MISTRAS series PCI AE system. The system has a high monitoring data stability and good monitoring effect under complicated noise interference. It can extract data parameters instantaneously and perform further processing of waveforms. The system uses an 18-bit A/D conversion digital signal processing module, which can realize instantaneous six-channel acquisition of the AE signal released by the sample during the loading process of the test. The threshold of the AE channel is 40 dB, and the threshold of the amplitude is 6 dB. The amplifier gain is 40 dB, the sensor resonance frequency is 20~100 kHz, and the data acquisition frequency is $10^6$ times/s. The test loading control system is shown in Fig. 2. During the loading process, a Canon professional high-speed camera is used to record the surface crack propagation process of the specimen.

## 3. Analysis of test results

### *3.1 Failure characteristics and crack evolution of rock with multiple defects in different loading stages*

In this paper, the initiation stress and the peak stress are regarded as two characteristic stress points. As shown in Fig. 3, the crack evolution process of the selected representative sample is divided into three stages for comparative analysis: the incipient cracking stage (0~$t_1$, the stress reaches crack initiation stress, that is, crack initiation occurs in the specimen), intermediate extension stage ($t_1$~$t_2$, the stress reaches peak, the specimen crack extension and connection), and late transfixion stage ($t_2$~$t_3$, the specimen failure), corresponding to $t_1$ (the crack shown in the red line), $t_2$ (the crack shown in the green line) and $t_3$ (the crack shown in the yellow line) in Fig. 3. The statistics of the crack type and crack extension angle (the small angle between the crack and the horizontal end surface) of the representative sample in Fig. 3 are shown in Table 1. Due to space limitations, this paper selects $\alpha$=30° samples for empirical analysis. Observing Fig. 3 (a), we obtain the following findings:

Incipient cracking stage: The specimen was loaded to 2.06 MPa (time is 66 s), which was approximately 12.8% of the peak stress, that is, at time $t_1$, the first stress drop point appears on the stress curve, and the specimen emits sound due to brittle deformation. Then, cracks A-1 and a few connecting holes A-2 were generated on the lower end face of the specimen. When A-1 expanded by 2 mm along the direction parallel to the external load, it rapidly connected with the top hole of the cavity group along the direction approximately 60° with the lower end face, and the connected direction was perpendicular to the boundary of the hole. After the initiation of the A-2 crack, it propagated approximately parallel to the 30° dip angle of the cavity group.

Table 1 Data of crack types and crack extension angles of different cavity group angles

| Cavity Group Angle | Types of Crack | Crack Extension Angle (°) |
|---|---|---|
| α=30° | tensile crack (A-1, A-3, A-4), shear crack (A-2) | 63.2 (A-1), 32.1 (A-2), 88.9 (A-3), 87.6 (A-4) |
| α=45° | tensile crack (A-1, A-2, A-3, A-4) | 89.6 (A-1), 78.8 (A-2), 84.6 (A-3), 88.2 (A-4) |
| α=60° | tensile crack (A-2, A-3, A-4), shear crack (A-1) | 59.3 (A-1), 83.9 (A-2), 76.1 (A-3), 3.2 (A-4) |
| α=75° | tensile crack (A-2, A-3, A-5, A-6), shear crack (A-1, A-4) spalling crack (B-1, B-2) | 77.8 (A-1), 84.6 (A-2), 88.5 (A-3), 65.2 (A-4)77.6 (A-5), 88.2 (A-6) |

Intermediate extension stage: As the load further increases, it reaches $t_2$, that is, the load reaches the peak stress of 16.14 MPa. At this time, the stress curve drops rapidly, and then the stress curve fluctuates intensively. A-1 continues to expand and then connects the front end of the strip-shaped through-going crack, A-2 extends approximately 26 mm along the direction parallel to the dip angle of the cavity group at 30° and immediately turns to continue to expand to the strip-shaped through-going crack in the direction parallel to the external load. At the same time, two A-3 cracks were generated along a principal stress direction in the upper part of the strip-shaped through-going crack, and both of these cracks were nearly perpendicular to the strip-shaped through-crack plane after expansion. On one side of the specimen containing the strip-shaped through-going crack, a crack was generated and propagated through the whole specimen, and the overall strength decreased significantly for the first time.

Late transfixion stage: The loading continues, and when $t_3$ is reached, the cracks between the cavities in the cavity group begin to initiate and develop, and the initiation direction is approximately perpendicular to the boundary of the cavity group. The cracks among the cavity group in the rock sample with an inclination angle of 30° are approximately parallel to the direction of external loading and develop independently with almost no connection between each other. However, micro-fractures that connect to the strip-shaped through-going cracks are still produced at the top of the cavity group. At the same time, A-4 along the principal stress direction is derived from the lower section of A-1, which quickly extend to the upper end and the right end of the specimen, respectively, resulting in cracks that cut across the specimen, which leads to tensile damage to the specimen.

The results show that the crack propagation laws of specimens with different cavity group inclinations exhibit clear stage characteristics. By summarizing the crack evolution path of the four groups of specimens in Fig. 3, we can obtain the following results:

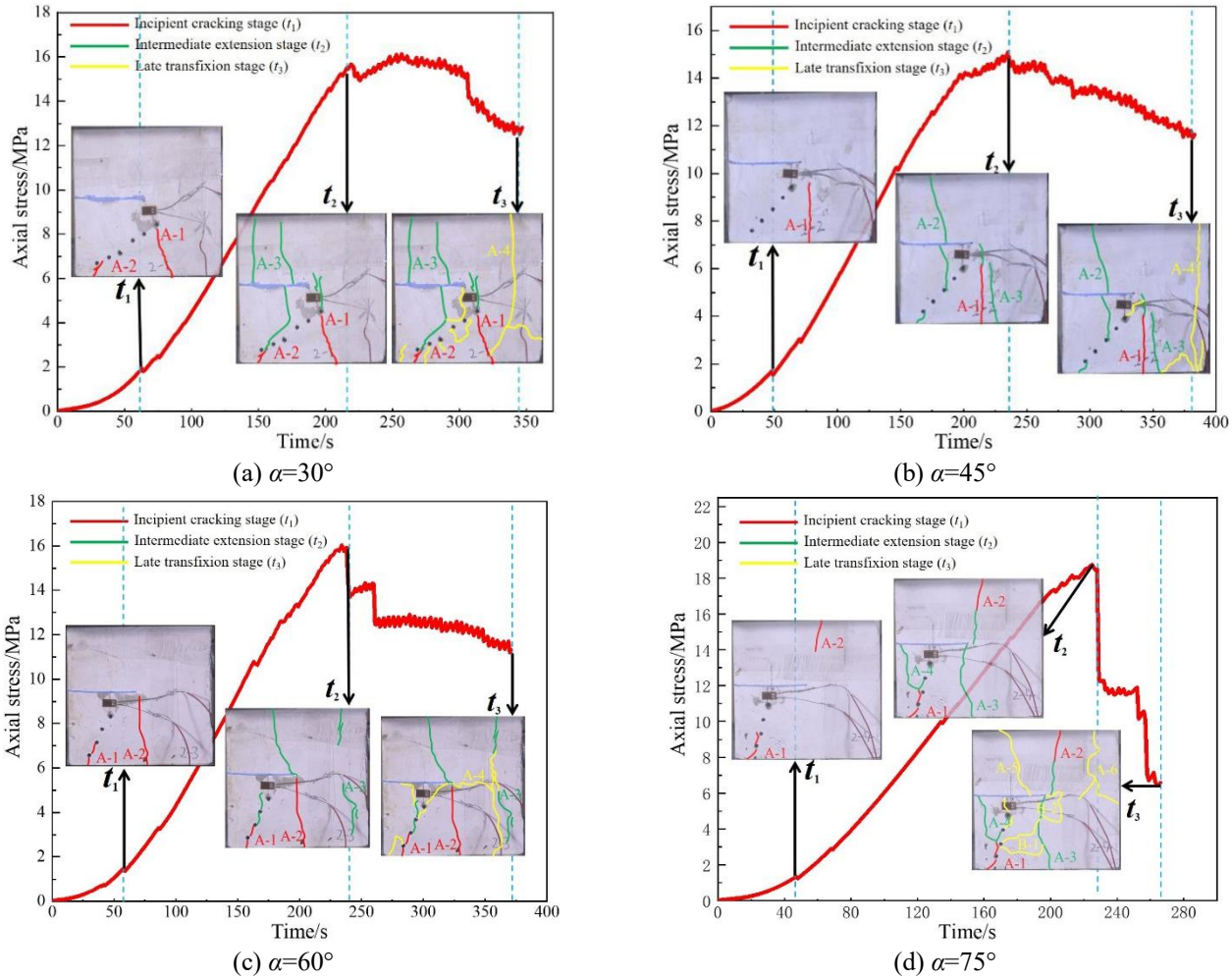


Fig. 3 Detailed diagram of the evolution process of cracks in defective rock samples with different cavity group inclinations

In the initial stage of cracking, the hoop effect remaining at the end has a certain influence on the crack initiation of the specimen, making the cracking initiation direction approximately 90° to the strip-shaped through-going cracks. However, Fig. 4 shows that when the cavity group inclination is larger, the crack initiation stress of the specimen decreases obviously. In addition, the time for the first crack to form in the specimen is gradually reduced. This shows that the increase in the cavity group inclination causes the initial damage of the rock with multiple defects to form more easily, resulting in the decrease in the initial crack initiation stress and crack initiation time.

In the middle stage of crack propagation, crack A-1 rapidly extended and expanded to connect with the strip-shaped through-going crack, and a few short tensile cracks were generated on both ends of the strip-shaped through-going crack, which basically formed through-going cracks centred on the front end of the strip-shaped through-going crack. It can be seen that with the increase in the cavity group inclination, the relationship between the crack development and the cavity group strengthens, and the shear cracks between the cavities in the cavity group increase significantly. For example, when the inclination angle $\alpha$ is 30°, cracks will grow between the cavities in the cavity group, but they develop relatively independently along the direction parallel to the external load; when the

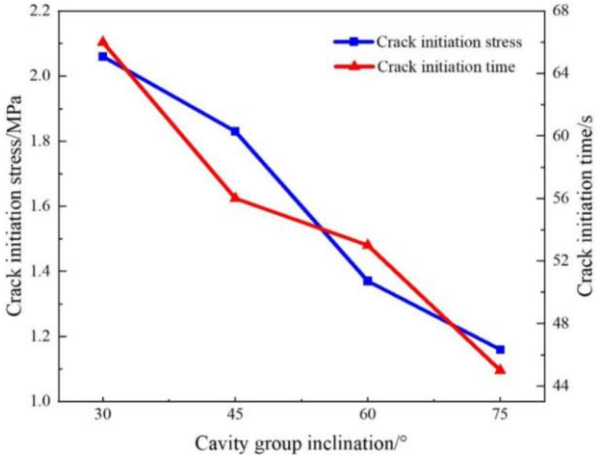


Fig. 4 Crack initiation stress and time under different cavity group inclination angles

inclination angle $\alpha$ is 45°, a few holes will initiate cracks, and the crack development direction between the bottom and top of the cavity group is approximately 45°; when the inclination angle $\alpha$ is 60°, the cracks between the cavities in the cavity group can interpenetrate, and the development direction is almost parallel to the inclination of the cavity group; when the inclination angle

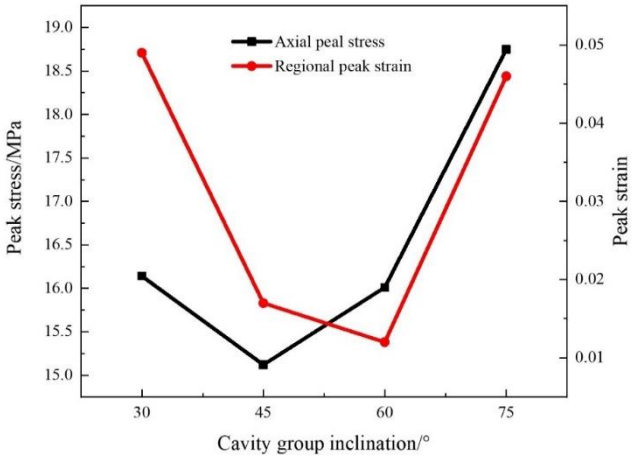


Fig. 5 Peak stress-strain diagram under different cavity group inclinations

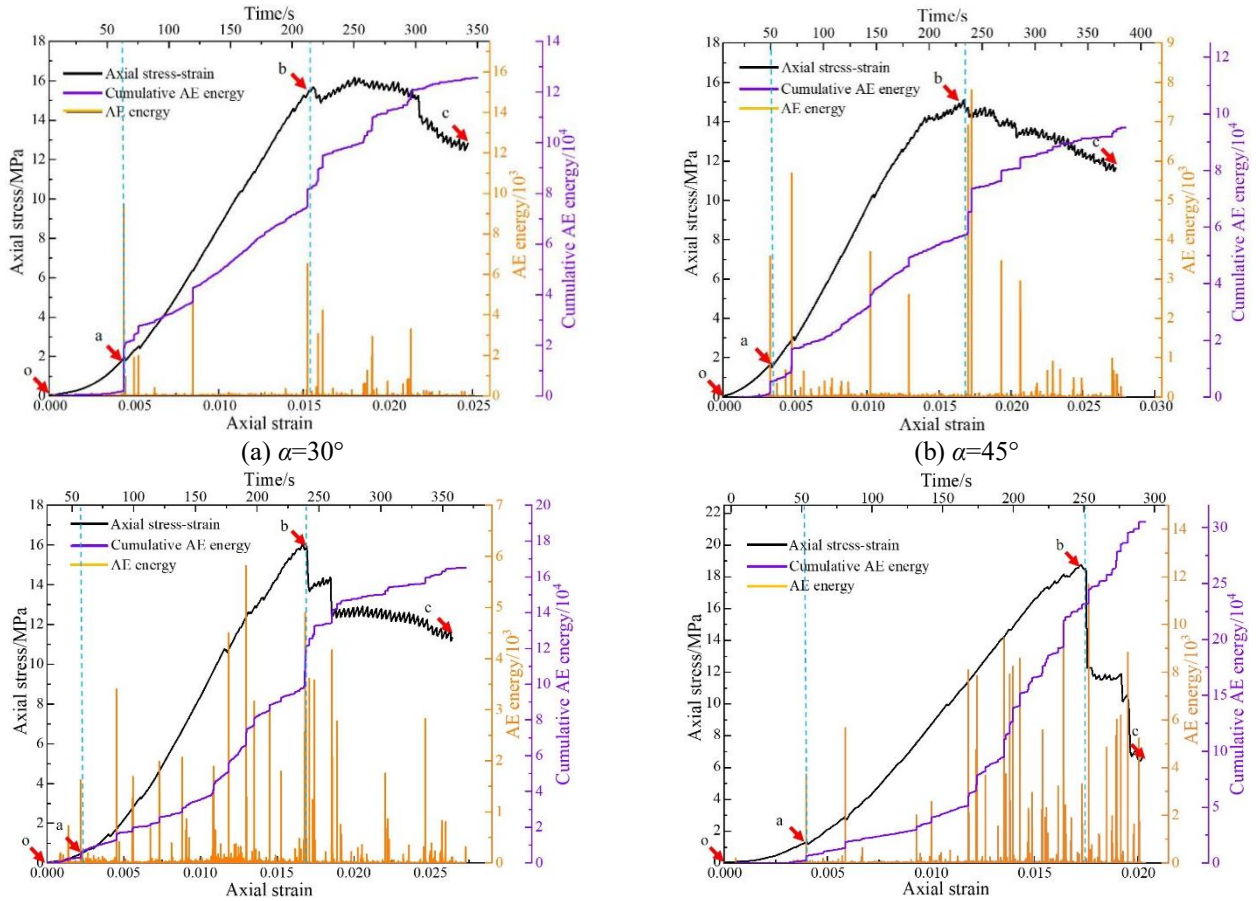


o-a compaction stage; a-b initiation stage to expansion stage; b-c late interpenetrating damage stage

Fig. 6 AE curve of axial stress and axial strain under different cavity group inclinations of defective rock samples

$\alpha$ is 75°, the cracks between the cavities in the cavity group not only extend along the inclination of the cavity group but also obviously, powdery debris is generated between the cavities in the cavity group. Slight slip failure occurs bear the holes in the sample under the shear mechanism, as shown in Fig. 3(d).

When entering the later stage of interpenetration, the specimens can basically form tensile cracks throughout the whole specimen, resulting in tensile failure. The statistics of the fracture lengths of rock samples at various angles show that when the inclination of the cavity group is 30°, the number of large-scale fractures exceeding 25 mm is twice as high as that when the inclination of the cavity group is 75°. Although the fracture modes of the 60° and 75° rock samples are basically the same, the difference is that the small-scale cracks are more developed and the crack lengths are shorter in the 75° rock sample than those in the 60° rock sample. This is basically consistent with the change law

reflected by the gradual intensive generation of AE energy in Fig. 6, that is, the sudden increase in the AE energy at a small angle is accompanied by the occurrence of large-scale cracks, and as the angle increases, the AE energy appears densely distributed, and the cumulative AE energy curve continues to increase rapidly. Although more cracks are produced in the process of failure, most of them are small-scale cracks less than 25 mm.

The surface cracks of the specimen are mainly in the form of tensile cracks and local shear cracks. The main features of the tensile crack are as follows: wide distribution, large proportion, crack initiation angle of approximately 90°, and extension angle of approximately 75~90° from the prefabricated strip-shaped through-going crack, as shown in Fig. 3(a) (A-3). With the enhancement of loading, the propagation angle gradually becomes parallel to the loading direction, and the crack opens. The local shear cracks are mainly distributed between the cavities in the cavity group, and the extension angle is approximately along the inclination of the cavity group. The cracks appear as obvious shear slip marks, accompanied by a small amount of rock dust, as shown in Fig. 3(d) (A-1). When the initial crack is connected with the tip of the prefabricated strip-shaped through-going crack, the phenomenon of "flake off" occurs at the tip of the prefabricated strip-shaped through-going crack, as shown in spalling area B-2 in Fig. 3 (d). The reason for this finding is that under the action of compressive stress, the rock above the prefabricated strip-shaped through-going crack bends, and the tip of the prefabricated strip-shaped through-going crack becomes the turning fulcrum, which leads to the phenomenon of "flake off". However, when the load reaches the peak stress, tensile failure still occurs, so the specimen is likely to fail in tension, but shear cracks accelerate its failure rate.

### *3.2 Analysis of AE characteristics of rock-like specimens*

Ultrasonic, X-ray and SEM (scanning electron microscopy) techniques are often used in the detection of rock defects. In real-time rock test, these techniques generally cannot be continuously monitored, so they have some limitations and deficiencies. However, AE technique can detect dynamic defects such as fracture and crack propagation of rock. Therefore, AE energy is widely used in rock mechanics tests as a characteristic parameter to identify the strength and weakness of rock fracture signals. Fig. 6 shows the curves of the axial stress and strain, AE energy and cumulative AE energy of the specimen at various angles. In Fig. 6, it can be seen that with the increase in the inclination of the cavity group, the AE energy distribution curve of each specimen shows the phenomenon of progressive denseness; that is, the AE signal recognition gradually transitioned from intermittent activity that occurred after long intervals of quiet to intensive activity that occurred after short intervals of quiet, the axial stress-strain curve fell increased faster, and the brittleness of the rock became increasingly prominent.

Fig. 6 shows that the axial stress-strain curve of each specimen has a good correspondence with AE energy and generally has obvious stage-specific characteristics. In the compaction stage, the AE signal is weak, which is mainly manifested as the closure of cracks inside the rock, accompanied by a very small number of microcracks. Subsequently, the rock entered the initial fissure initiation stage, and some micro-fractures developed in the rock. The first observable fracture appeared on the rock surface, the AE energy showed a sharp rise accompanied by a cluster of low-energy events, and the cumulative AE energy curve shows an obvious step-like climb. However, with the increase in the angle of the cavity group, the specimens show obvious differences during the elastic stage, that is, with the increase in the angle of the cavity group, the total amount of AE signals and energy increase significantly during this stage, and as the slope of the cumulative AE energy curve increases continuously, from $7.74\times10^4$ at 30° to $24.93\times10^4$ at 75°, the cumulative AE energy increases by approximately 3.2 times. The reason for this phenomenon is as described in section 3.1. As the inclination angle of the cavity group increases, the relationship between crack development and the cavity group becomes increasingly close, and the cracks between the cavities in the cavity group increase significantly, which makes the cavity group slip along the fracture surface, resulting in abnormal AE activity for samples with a large cavity group inclination angle. For the sample with a small cavity group inclination angle, Fig. 6(a) shows that except for the sudden rise in AE energy when macrofractures are generated, the AE energy is in a relatively calm period at other times, and the fractures expand stably.

When the rock sample enters the later stage of interpenetration, Figs. 6(c) and 6(d) can hardly distinguish the boundary of the fracture stage from only the AE energy curve, as shown in Figs. 6(a) and 6(b). However, it can be observed from the stress-strain curves in both Figs. 6(c) and 6(d) that a large stress drop occurs. In the experiment, the peak strength in Fig. 6(d) dropped from 18.75 MPa to 6.43 MPa, a decrease of 12.32 MPa or 65.7%. In this stage, the strain increased by 0.23%, accounting for approximately 1/8 of the total strain, and the post-peak drop characteristics are more significant. The analysis shows that the stress-strain curve of the large-angle sample has a step-down phenomenon, which indicates that the bearing capacity of the sample decreases, and severe damage occurs in local areas. However, the failure of the local area does not lead to the complete loss of the bearing capacity of the sample, so the lag in the drop in the stress-strain curve shows a slow zigzag decline.

To explore the influence of the change in cavity group inclination on the cumulative AE event count of specimens, the length $l$ of the horizontal control area of the cavity group was introduced to express this influence quantitatively.

$$l=2d\cos\alpha$$

In the formula, $d$ is the length of half of the line between the top and bottom of the cavity group along the centre of the holes, mm, and $\alpha$ is the inclination angle of the cavity group. Taking line AB, which is parallel to the end face and is the axis of rotation symmetry of the cavity group, the cavity group is projected on the line segment AB, where $l$ is the length of the horizontal control area of the cavity group,

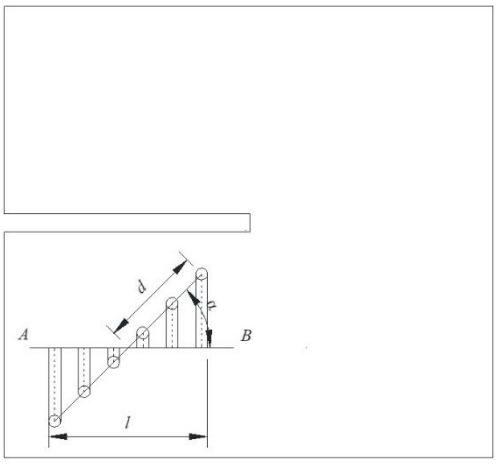


Fig. 7 Length of the horizontal control area of the cavity group

Table 2 Statistics of deformation stages under different cavity group inclinations

| α (°) | l (mm) | Proportion of Stage o-a (%) | | Proportion of Stage a-b (%) | | Proportion of Stage b-c (%) | | ΣE ($10^4$) | ΣN ($10^4$) |
|---|---|---|---|---|---|---|---|---|---|
| | | Time | Event | Time | Event | Time | Event | | |
| 30 | 30.31 | 18.22 | 3.03 | 42.46 | 74.71 | 39.32 | 22.26 | 12.86 | 17.18 |
| 45 | 19.8 | 12.49 | 2.59 | 48.8 | 81.03 | 38.71 | 16.38 | 9.73 | 12.56 |
| 60 | 10.5 | 17.04 | 6.61 | 47.37 | 82.53 | 35.59 | 10.86 | 16.69 | 18.76 |
| 75 | 5.44 | 16.26 | 1.84 | 70 | 86.07 | 13.74 | 12.09 | 31.24 | 21.2 |

as shown in Fig. 7. The length of the horizontal control area, the proportion of the stage duration, the proportion of the cumulative AE event in each stage, the cumulative AE energy ΣE, and the cumulative AE event count ΣN are listed in Table 2.

As seen from the data in Table 2, the cumulative AE event count proportion of the sample during the compaction stage of o-a is small, and the rock sample has almost no damage. When loading continues and enters stages a-b, the cumulative AE event count starts to show certain regularity with the change in the cavity group inclination, that is, the event count shows a gradual increase with the increase in cavity group inclination in this stage. When the inclination angle of the cavity group reaches 75°, the event count accounts for 86.07%, indicating that the damage in the local area of the hole is more active under the condition of the larger cavity group inclination during this stage, resulting in more damage, which has the trend of dominating the whole fracture process. However, during the later stage of interpenetration of b-c, it could be observed that the time proportion of large-angle samples began to decrease significantly, and the stress-strain curve in Fig. 6 shows that the stress drop and brittleness increased remarkably, while the residual bearing capacity decreased.

In addition, it can be seen from Table 2 that although the cumulative AE energy ΣE and the cumulative AE event count ΣN are different in magnitude, the overall change trends are basically the same, that is, as the inclination of the cavity group increases, the length of the horizontal control area of the cavity group decreases, and the cumulative AE energy ΣE and cumulative AE event count ΣN are bounded by the inclination angle of the cavity group at 45°, showing a trend of first decreasing and then increasing. Combined with the peak stress in Fig. 5, it can be seen that the axial peak stress diagram has a similar change trend with the cumulative AE energy ΣE and cumulative AE events count ΣN. This is because with the decrease in the length of the horizontal control area of the cavity group, the scope of the horizontal control of the cavity group decreases relative to the specimen as a whole, and the fracture mode of the specimen gradually changes from the integral rupture mode to the shear slip mode along the dip angle of the cavity group in the local area. Therefore, the sample has a higher degree of fracture, and more AE signals are collected. However, when the inclination angle of the cavity group is 45°, the axial peak stress, the cumulative AE energy ΣE, and the cumulative AE event count ΣN all show the smallest values obtained. The main reason for this result is as follows: when there are multiple defects, the crack propagation is affected by both the cavity group and the strip-shaped through-going crack. When the angle of the cavity group is 45°, the cubic structure of the specimen is more likely to cause general shear failure and cracks, and the points of intersection between the extension line of the cavity group and the front end of the strip-shaped through-going crack are closest to the high stress area around the strip-shaped through-going crack, making the specimen more likely to be destroyed under compression, so the degree of rupture in the local area is relatively small, and the number of AE signals recorded also decreases accordingly.

### *3.3 Analysis of rock-like deformation characteristics*

To plot the axial stress-time-local strain curve, as shown in Fig. 8, the local strain is collected by the strain sensor. It can be seen from the figure that the four sets of samples clearly undergo compression during the closing stage I, elastic deformation stage II, rupture and yield stage III and softening stage IV.

The stress-strain curves corresponding to the cavity group inclination angles of 30° and 45° did not show a large stress drop after reaching the peak stress in the rupture and yield stage, but a yield platform appeared, clearly showing a plastic flow phenomenon. When the inclination angle of the cavity group reaches 60°, the sample clearly exhibits a stepped stress drop after the peak stress. The peak stress drops from 16.03 MPa to 12.47 MPa, which is a decrease of 3.56 MPa, or 22.2%, and the strain in this stage increases by 1.5%. When the inclination angle of the cavity group reaches 75°, the vertical stress drop of the stress-strain curve is more obvious after reaching the peak stress, reaching 65.7%. Compared with the results for other angles, the residual bearing capacity of the rock sample decreases more at this angle, which means that with the increase in the inclination of the cavity group, the fracture degree of the sample surface after the softening stage becomes increasingly severe, the plasticity of the rock gradually weakens, and the fracture mode shows a transition trend from plastic failure to brittle failure. The reason for these

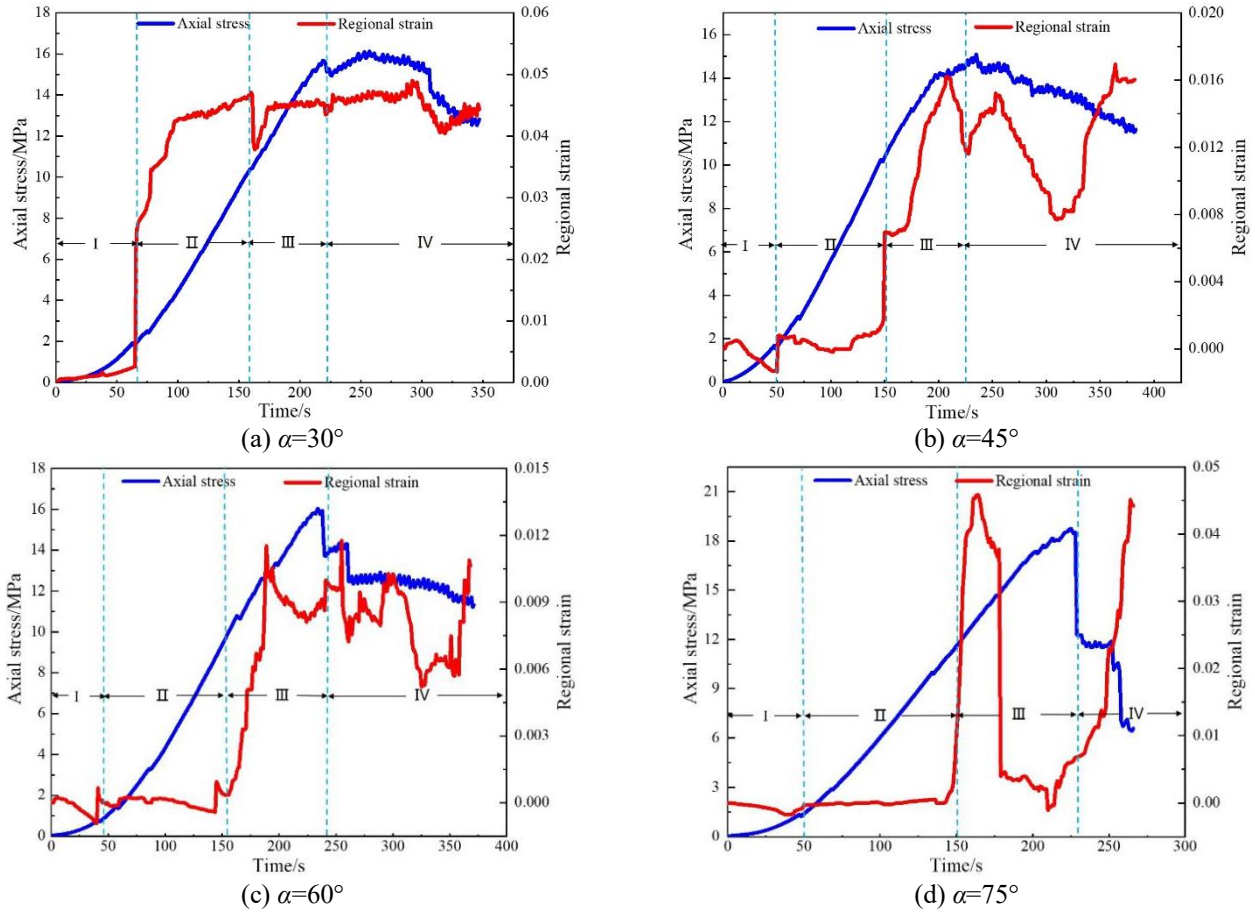


(a) $\alpha$=30° (b) $\alpha$=45°

(c) $\alpha$=60° (d) $\alpha$=75°

Fig. 8 Local strain curve of axial stress under different cave group inclinations of the defective rock sample

trends is that as the inclination angle of the cavity group increases, the shear cracks between the cavities in the cavity group aggravate the slip and wear between the holes under the action of the external load, resulting in stress concentration, so that the shear cracks between the cavities in the cavity group are more easily connected with the tensile cracks. As a result, the energy accumulated by the specimen under compression can be released suddenly, resulting in deformation mutation and greater brittleness. The phenomenon of "flake off" in Fig. 3 provides strong proof of this conclusion. Therefore, the change in the inclination angle of the cavity group is quite sensitive to the influence of the rock mass properties in actual engineering, and a large inclination angle of a cavity group defect structure in a rock mass should be avoided to prevent the sudden failure of the rock mass.

The strain gauge mentioned above is used to monitor the local deformation in this area. The analysis can be obtained from Fig. 8(a). The strain gauge monitoring area of a specimen under uniaxial compression is mainly affected by the tensile stress perpendicular to the axial stress direction. When the specimen reaches the initiation stress of 2.06 MPa, the strain in the local area increases sharply and then reaches the strain peak. The reason for this result is that the crack A-1 of the specimen rapidly expanded to the top of the cavity group after the crack started and then developed into an intersecting crack with the high-stress area at the tip of the strip-shaped through-going crack, resulting in a rapid

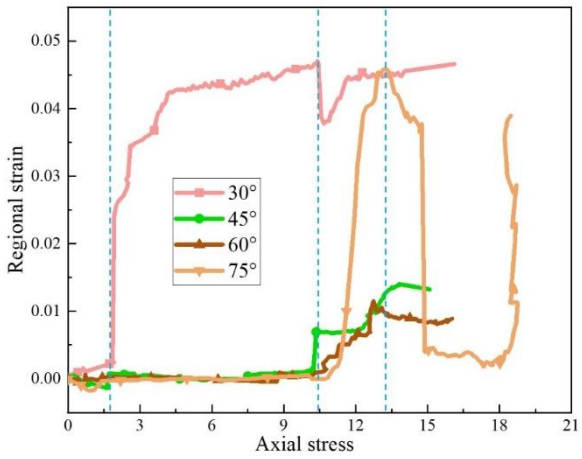


Fig. 9 Regional strain-axial stress curve

increase in the tensile strain within the local area. Under uniaxial compression, the specimens with cavity group inclination angles of 45°, 60° and 75° exhibited a small tensile stress perpendicular to the axial stress direction in the early stage of the strain gauge monitoring area. With loading, the stress changed from tensile stress to compressive stress and then fluctuated between compressive stress and tensile stress. With a further increase in the load, it appears that the monitoring area was mainly subjected to tensile stress perpendicular to the axial stress direction. The reason for this result is that the distance

between the tip of the strip-shaped through-going crack and the top of the cavity group is greater, which causes the effective force area in the local area to increase, and the compressive stress environment formed later is more conducive to suppressing the growth of cracks, resulting in a small fluctuation in the local strain in a considerable period of time.

Although the axial stress-time-local strain curves of specimens with cavity group inclination angles of 75° were partially consistent with those of specimens with cavity group inclinations of 45° and 60° in the early stage, there were two obvious large fluctuations in the later stage. It can be seen from Fig. 9 that the local peak strain ($4.6\times10^{-2}$) of the specimen with a cavity group inclination angle of 75° reaches the local peak strain ($4.9\times10^{-2}$), which is similar to that of the specimen with a 30° cavity group inclination, indicating that when the inclination angle of the cavity group is 30° or 75°, the specimen is more likely to form cracks under the tensile stress in the monitored local area than under the conditions of 45° and 60°. The main reason for this phenomenon is that when the cavity group inclination angle is close to 0°, the length of the horizontal control area of the cavity group increases greatly, and the defects increase in the same horizontal plane, which may decrease the bearing capacity of the specimen. When the cavity group inclination angle is close to 90°, the cracks between the cavities in the cavity group can slip along the inclination angle of the cavity group under the shear mechanism, resulting in the failure of the monitoring local area due to tension. In view of this experimental phenomenon, the excavation of caverns with too large or too small inclination angle should be minimized as far as possible in engineering practice, so as to avoid the crack propagation in local area, and then connect the confined water aquifer to form a water inrush channel, leading to flood. Entering the intermediate extension stage, the tendency of cracks A-2 and A-3 to interpenetrate is the main reason for the sharp rise in the strain in the local area, and the second fluctuation is due to the phenomenon of "flake off" in the monitoring area caused by strain gauge failure.

## 4. Conclusions

This work used a Shimadzu AG-X250 rock testing machine and AE system to conduct uniaxial compression tests and AE tests on prefabricated rock specimens with multiple defects, analysing the influence of the change in the inclination angle of the cavity group on the crack propagation and deformation and failure characteristics of the specimen. In addition, based on the characteristics of the AE signal, the differences in the fracture mechanisms of rock samples in different test scenes were compared. Finally, with the help of the DH-3816N strain acquisition system, the variation in the area between the strip-shaped through-going crack defects and the cavity group defects was studied. The main conclusions are as follows:

• The cracks evolution process of the specimen with strip-shaped through-going cracks and cavity groups has obvious stage characteristics after compression. The change of the cavity group inclination angle has an effect on the crack initiation stress and crack initiation time at the incipient cracking stage.

• As the angle of α increases its relationship with crack development tends to strengthen, and more small-scale and densely distributed shear cracks between the cavity group are the main reasons for the interconnection of the cavities.

• The crack initiation angle of tensile cracks has obvious regularity, and such cracks play a major role in the fracture mode of rock. After the initial crack propagation, it is generally connected at the tip of the prefabricated strip-shaped through-going crack. At this time, the specimen will be cracked into an independent bearing unit, resulting in the possibility of bending of the rock above the prefabricated strip-shaped through-going crack, which has a great impact on the failure of the specimen.

• The evolution law of the AE signal parameters of each sample is in good agreement with the trend of the stress-strain curve, and the frequency of AE energy fluctuation at the peak stress is generally higher than that at other times.

• With the increase in the inclination angle of the cavity group, the length of the horizontal control area of the cavity group decreases linearly, but the cumulative AE energy and the cumulative AE event count first decrease and then increase. When the inclination angle of the cavity group is 45°, the weakening of both values is the greatest.

• When the cavity group inclination angle is close to 0° or 90°, showing that cracks easily occur in the local area at this angle, and the cracks further develop, weakening the overall strength of the rock, and increasing the probability of damage to the engineering quality.

• The research content of this paper mainly focuses on a comparison of rock samples with various cavity group inclinations, while the influence of the prefabricated strip-shaped through-going cracks on the edge is only preliminarily discussed. In the next step, the mechanical properties of samples with different lengths of strip-shaped through-going cracks and different cavity group shapes will be investigated to provide theoretical support for underground engineering construction, such as tunnels and chambers.

## Conflicts of interest

The authors declare that they have no known competing financial interests or personal relationships that could have appeared to influence the work reported in this paper.

## Acknowledgments

This research was financially supported by the National Natural Science Foundation of China (Grant No. 51804179; 52004147 and 51974173), Natural Science Foundation of Shandong Province (Grant No. ZR2020QE129), Key Research and Development Plan of Shandong Province (Grant No. 2018GSF120003 and 2019GSF111024) and Shandong Province's Taishan Scholar Talent Team Support Plan for Advantaged & Unique Discipline Areas.

## References

Aalianvari, A. (2017), "Combination of engineering geological

data and numerical modeling results to classify the tunnel route based on the groundwater seepage", *Geomech. Eng.*, **13**(4), 671-683. https://doi.org/10.12989/gae.2017.13.4.671.

Alitalesh, M., Yazdani, M., Fakhimi, A. and Naeimabadi, M. (2020), "Effect of loading direction on interaction of two pre-existing open and closed flaws in a rock-like brittle material", *Undergr. Sp.*, **5**(3), 242-257. https://doi.org/10.1016/j.undsp.2019.04.003.

Bahaaddini, M., Sharrock, G. and Hebblewhite, B.K. (2013), "Numerical direct shear tests to model the shear behaviour of rock joints", *Comput. Geotech.*, **51**, 101-115. https://doi.org/10.1016/j.compgeo.2013.02.003.

Dyskin, A.V., Sahouryeh, E. and Jewell, R.J. (2003), "Influence of shape and locations of initial 3-D cracks on their growth in uniaxial compression", *Eng. Fract. Mech.*, **70**(15), 2115-2136. https://doi.org/10.1016/S0013-7944(02)00240-0.

Dzik, E.J. and Lajtai, E.Z. (1996), "Primary fracture propagation from circular cavities loaded in compression", *Int. J. Fracture*, **79**(1), 49-64. https://doi.org/10.1007/BF00017712.

Fan, X., Chen, R. and Hang, L. (2018), "Cracking and failure in rock specimen containing combined flaw and hole under uniaxial compression", *Adv. Civ. Eng.* https://doi.org/10.1155/2018/9818250.

Golewski, G.L. (2019), "A new principles for implementation and operation of foundations for machines: A review of recent advances", *Struct. Eng. Mech.*, **71**(3), 317-327. https://doi.org/10.12989/sem.2019.71.3.317.

Golewski, G.L. (2019), "A novel specific requirements for materials used in reinforced concrete composites subjected to dynamic loads", *Compos. Struct.*, **223**, 110939. https://doi.org/10.1016/j.compstruct.2019.110939.

Golewski, G.L. and Sadowski, T. (2016), "A study of mode III fracture toughness in young and mature concrete with fly ash additive", *Solid State Phenom.*, **254**, 120-125. https://doi.org/10.4028/www.scientific.net/SSP.254.120.

Gongzalez-Quiros, A. and Fernandez-Alvarez, J.P. (2019), "Conceptualization and finite element groundwater flow modeling of a flooded underground mine reservoir in the Asturian Coal Basin, Spain", *J. Hydrol.*, **578**. https://doi.org/10.1016/j.jhydrol.2019.124036.

Haeri, H., Khaloo, A. and Marji, M.F. (2015), "Fracture analyses of different pre-holed concrete specimens under compression", *Acta Mech. Sinica*, **31**(06), 855-870. https://doi.org/10.1007/s10409-015-0436-3.

Haeri, H., Shahriar, K. and Marji, M.F. (2014), "Experimental and numerical study of crack propagation and coalescence in pre-cracked rock-like disks", *Int. J. Rock Mech. Min. Sci.*, **67**, 20-28. https://doi.org/10.1016/j.ijrmms.2014.01.008,

Jaime, M.C., Zhou, Y.N. and Lin, J.S. (2015), "Finite element modeling of rock cutting and its fragmentation process", *Int. J. Rock Mech. Min. Sci.*, **80**, 137-146. https://doi.org/10.1016/j.ijrmms.2015.09.004.

Jin, J., Cao, P. and Chen, Y. (2017), "Influence of single flaw on the failure process and energy mechanics of rock-like material", *Comput. Geotech.*, **86**, 150-162. https://doi.org/10.1016/j.compgeo.2017.01.011.

Kadomtsev, A.G., Damaskinskaya E.E. and Kuksenko V.S. (2011), "Fracture features of granite under various deformation conditions", *Phys. Solid State*, **53**(9), 1876-1881. https://doi.org/10.1134/S1063783411090150.

Kong, X.G., Wang, E.Y. and He, X.Q. (2018), "Cracks evolution and multifractal of acoustic emission energy during coal loading", *Geomech. Eng.*, **14**(2), 107-113. https://doi.org/10.12989/gae.2018.14.2.107.

Kulatilake, P.H.S.W., Malama, B. and Wang, J.L. (2001), "Physical and particle flow modeling of jointed rock block behavior under uniaxial loading", *Int. J. Rock Mech. Min. Sci.*, **38**(5), 641-657. https://doi.org/10.1016/S1365-1609(01)00025-9.

Lee, H. and Jeon. S. (2010), "An experimental and numerical study of fracture coalescence in pre-cracked specimens under uniaxial compression", *Int. J. Solids Struct.*, **48**(6), 979-999. https://doi.org/10.1016/j.ijsolstr.2010.12.001.

Liang, Z.Z., Xing, H. and Wang, S.Y. (2012), "A three-dimensional numerical investigation of the fracture of rock specimens containing a pre-existing surface flaw", *Comput. Geotech.*, **45**, 19-33. https://doi.org/10.1016/j.compgeo.2012.04.011.

Lyer, K. and Podladchikov, Y.Y. (2009), "Transformation-induced jointing as a gauge for interfacial slip and rock strength", *Earth Planet Sci. Lett.*, **280**(1-4), 159-166. https://doi.org/10.1016/j.epsl.2009.01.028.

Madkour, H. (2012), "Parametric analysis of tunnel behavior in jointed rock", *Ain Shams Eng. J.*, **3**(2),79-103. https://doi.org/10.1016/j.asej.2012.01.002.

Mejia Camones, L.A., Vargas Jr, E.d.A., Figueiredo, R.P. and Velloso R.Q. (2013), "Application of the discrete element method for modeling of rock crack propagation and coalescence in the step-path failure mechanism", *Eng. Geol.*, **153**, 80-94. https://doi.org/10.1016/j.enggeo.2012.11.013.

Moir, H., Lunn, R.J. and Shipton, Z.K. (2009), "Simulating brittle fault evolution from networks of pre-existing joints within crystalline rock", *J. Struct. Geol.*, **32**(11), 1742-1753. https://doi.org/10.1016/j.jsg.2009.08.016.

Mondal, S., Olsen-Kettle, L. and Gross, L. (2019), "Simulating damage evolution and fracture propagation in sandstone containing a preexisting 3-D surface flaw under uniaxial compression", *Int. J. Numer. Anal. Met.*, **43**(7), 1448-1466. https://doi.org/10.1002/nag.2908.

Oh, J., Moon, T., Canbulat, I. and Moon, J.S. (2019), "Design of initial support required for excavation of underground cavern and shaft from numerical analysis", *Geomech. Eng.*, **17**(6),573-581. https://doi.org/10.12989/gae.2019.17.6.573.

Qian, Q.H. and Zhou, X.P. (2018), "Failure behaviors and rock deformation during excavation of underground cavern group for Jinping I Hydropower Station", *Rock Mech. Rock Eng.*, **51**(8), 2639-2651. https://doi.org/10.1007/s00603-018-1518-x.

Shemirani, A.B., Haeri, H. Sarfarazi, V. and Hedayat, A. (2017), "A review paper about experimental investigations on failure behaviour of non-persistent joint", *Geomech. Eng.*, **13**(4), 535-570. https://doi.org/10.12989/gae.2017.13.4.535.

Shen, B.T., Siren, T. and Rinne, M. (2015), "Modelling fracture propagation in anisotropic rock mass", *Rock Mech. Rock Eng.*, **48**(3), 1067-1081. https://doi.org/10.1007/s00603-014-0621-x.

Vahab, S. and Hadi, H. (2016), "A review of experimental and numerical investigations about crack propagation", *Comput. Concrete*, **18**(2), 235-266. https://doi.org/10.12989/cac.2016.18.2.235.

Waltham, A.C. and Swift, G.M. (2004), "Bearing capacity of rock over mined cavities in Nottingham", *Eng. Geol.*, **75**(1), 15-31. https://doi.org/10.1016/j.enggeo.2004.04.006.

Winn, K., Wong, L.N.Y. and Alejano, L.R. (2019), "Multi-approach stability analyses of large caverns excavated in low-angled bedded sedimentary rock masses in Singapore", *Eng. Geol.*, **259**. https://doi.org/10.1016/j.enggeo.2019.105164.

Wong, R.H.C., Chau, K.T. and Tang, C.A. (2001), "Analysis of crack coalescence in rock-like materials containing three flaws—Part I: Experimental approach", *Int. J. Rock Mech. Min. Sci.*, **38**(7), 909-924. https://doi.org/10.1016/S1365-1609(01)00065-X.

Xu, S.D., Li, Y.H. and Liu, J.P. (2017), "Detection of cracking and damage mechanisms in brittle granites by moment tensor analysis of acoustic emission signals", *Acoust. Phys.*, **63**, 359-367. https://doi.org/10.1134/S1063771017030137.

Yang, S.Q. and Huang, Y.H. (2014), "Experiment and particle flow simulation on crack coalescence behavior of sandstone specimens containing double holes and a single fissure", *J. Basic Sci. Eng.*, **22**(03), 584-597. https://doi.org/10.3969/j.issn.1005-0930.2014.03.017.

Zeng, W., Yang, S.Q. and Tian, W.L. (2018), "Experimental and numerical investigation of brittle sandstone specimens containing different shapes of holes under uniaxial compression", *Eng. Fract. Mech.*, **200**, 430-450. https://doi.org/10.1016/j.engfracmech.2018.08.016.

Zhang, X.S. (2005), "Layout and monitoring-controlling design of underground openings and tunnels for Longtan Hydropower Station", *Chin. J. Rock Mech. Eng.*, **21**, 185-191. https://doi.org/10.1007/s11769-005-0030-x.

Zhou, Z.L., Tan, L.H. and Cao, W.Z. (2017), "Fracture evolution and failure behaviour of marble specimens containing rectangular cavities under uniaxial loading", *Eng. Fract. Mech.*, **184**, 183-201. https://doi.org/10.1016/j.engfracmech.2017.08.029.

*CC*